Surface Science 605 (2011) 1669–1675

Contents lists available at ScienceDirect

Surface Science

journal homepage: www.elsevier.com/ locate/susc

Folding and cracking of graphene oxide sheets upon deposition

Deepak K. Pandey [a,b,*], Ting Fung Chung [a,b], G. Prakash [a,b], R. Piner [c], Yong P. Chen [a,b], R. Reifenberger [a,b]

[a] Department of Physics, Purdue University W. Lafayette IN 47907, United States
[b] Brick Nanotechnology Center, Purdue University W. Lafayette IN 47907, United States
[c] Department of Mechanical Engineering, Mechanical Engineering Dept., The University of Texas at Austin, Austin, TX 78712-0292, United States

ARTICLE INFO

Available online 3 May 2011

ABSTRACT

Graphene Oxide (GO) sheets, suspended in an aqueous solution, were deposited on freshly cleaved highly oriented pyrolytic graphite (HOPG) and studied using Raman spectroscopy, atomic force microscopy (AFM) and scanning tunneling microscopy (STM). AFM phase imaging shows a distinct contrast between GO and the underlying HOPG substrate. Raman spectroscopy clearly showed the presence of GO sheets on the top of HOPG substrate. The AFM and STM images also reveal wrinkling, folding, and tearing of individual GO sheets after depositing onto an HOPG substrate. We have also observed a distinct cracking of a GO sheet after folding. We attribute this new cracking phenomenon to a weakening of C–C bonds during the oxidation of a graphene sheet.

1. Introduction

Since 2004 [1], the study of graphene has opened an entirely new domain in the area of 2D materials science and condensed matter physics to study and fabricate next generation low power electronics devices [2–5] and highly sensitive sensors [6–8]. Concurrently, thin sheets of GO have shown potential for use in novel carbon-based materials and provide an alternate path to graphene by reduction of GO [2–4,9–13]. The easy exfoliation of GO in a variety of solvents gives it an advantage over other existing methods for obtaining a single sheet of graphene in large quantities [9,10,12,14–16].

Tremendous amount of work is being done to better elucidate the structural, electronic, and chemical properties of GO. Recent theoretical [17,18] work [19] has demonstrated the presence of oxygen functional groups [C-O-C) on an individual GO sheet when deposited onto HOPG. Studies have indicated that GO, when deposited on a variety of substrates, acquires distinctive features that can be described as flat, wrinkled and folded [12,14]. Each feature suggests a potential use. Supported flat GO sheets are ideal for the fabrication of micro/nano electronic devices. Wrinkled GO sheets are relevant for biological sensor applications as it has been demonstrated that wrinkles in GO are favorable sites for biological agents to react [8].

GO has been recently studied and its structure is composed of carboxyl, hydroxyl and epoxy groups [20–23]. To better characterize GO, we studied this material using Raman spectroscopy as well as scanning probe microscopy methods. We have performed a series of experiments to understand the surface properties of individual GO sheets deposited onto HOPG. We present Raman, STM and AFM experiments performed under dry nitrogen conditions to study the morphology of single sheets of GO deposited onto an HOPG substrate. Our work shows that GO sheets tend to wrinkle and fold upon deposition from an aqueous solvent. In addition, we present new evidence that when folding; it is also possible for GO to crack. In what follows, we define *flat GO* as a sheet of GO that has no visible wrinkle, fold and/or crack, *folded GO* as a single sheet of GO folded onto itself and *cracked GO* as a single sheet of GO that cracks in the process of folding.

2. Synthesis of GO and sample preparation

The graphene oxide (GO) used in this study was synthesized from purified natural graphite (SP-1, Bay carbon) by the Hummers method [24]. The detailed procedure for preparation of GO sheets by chemical exfoliation method is discussed elsewhere [2,9,19].

HOPG was chosen as a substrate for depositing GO sheets because it provides an atomically flat base for deposition. A 1 cm × 1 cm substrate of highly-oriented pyrolitic graphite (HOPG) was first cleaved using scotch tape then a 2 μL drop of a solution containing GO sheets suspended in ultra pure water was deposited on this freshly cleaved HOPG. The drop covered the entire 1 cm^2 area of the HOPG substrate. The drop of GO deposited on HOPG was then placed in a covered Petri dish. After every 5 h, another drop of GO solution was deposited to prevent the drying of solution by evaporation. This process was continued for approximately 24 h to allow the GO sheets to adhere to the HOPG surface. After 24 h, the excess solution was wicked off from the HOPG substrate using lint free tissue paper to rapidly remove any salt or impurity present in the solution. This procedure was adopted rather than complete evaporation of the

* Corresponding author at: Department of Physics, Purdue University W. Lafayette IN 47907, United States. Tel.: +1 765 5867264.
E-mail address: dpandey@purdue.edu (D.K. Pandey).

0039-6028/$ – see front matter © 2011 Elsevier B.V. All rights reserved.
doi:10.1016/j.susc.2011.04.034

solution to reduce any impurities which might settle onto the GO sheets.

3. Experimental conditions

Three experimental set-ups, Raman, AFM and STM were used in this study. Raman spectroscopy is a widely used technique for characterizing carbon materials such as carbon nanotubes, graphite, graphene, and graphene oxide. The measurements were performed at room temperature with a Horiba XploRA Raman microscope with a 532 nm excitation laser and using a 2400 ln/mm grating and a 100× objective.

Topography and phase contrast AFM data were obtained under ambient pressures using a Nanotec AFM under dry nitrogen conditions. The images were acquired using the dynamic AFM (dAFM) mode. Silicon microcantilevers from Nanosensors (Model: PPP-NCLR) with nominal frequency 190 kHz and nominal stiffness 48 N/m. The dAFM scans were generally limited to areas of 3.5 μm × 3.5 μm or less with a typical scanning speed of 0.5 Hz. The dAFM images were acquired with setpoint amplitude of $0.6A_o$ where A_o is the free amplitude of cantilever's oscillation. Typically, we chose A_o to equal 15 nm.

The STM experiments were performed with a Nanotec Electronica STM under dry nitrogen environment. The tip used in the STM study was made of Pt/Ir and was freshly cut before every study. The gap (bias) voltage is applied to the sample with respect to the tip which is at ground potential. The bias voltage was + 0.5 V and the tunnel current was 1 nA. The STM scans were limited to areas of 3.5 μm × 3.5 μm or less.

4. Result and discussion

4.1. Raman study of graphene oxide sheets on HOPG

Raman spectra were obtained on GO sheets deposited on HOPG substrate (GO-HOPG). Careful analysis of Raman peaks confirmed the presence of GO on HOPG substrate. Fig. 1 presents the comparison of 532 nm Raman spectra of GO-HOPG (blue curve: color online) and bulk HOPG (red curve: color online). The prominent features of the bulk HOPG are the G band at ~1585 cm^{-1} and a 2D band at ~2700 cm^{-1} where as the disorder D bands caused by defects at ~1344 cm^{-1} as well as the asymmetric broadening of the G bands are the indication of GO-HOPG [25]. The absence of D band in the spectra of HOPG indicates the high quality defect-free bulk HOPG substrate. The appearance of the D band on GO-HOPG sheets with lateral dimensions much larger than the laser spot (~1um) signifies disorder in the carbon lattice, which is not due to edges of GO-HOPG sheets. The origin of disorder in the GO-HOPG sheets could be topological defects, vacancies and folding layers that may leave behind at GO transformation [26] and sample preparation[12,19]. Further analysis of G band of GO-HOPG also indicates asymmetric broadening at ~1585 cm^{-1} suggesting shift to higher frequencies (blue-shift), probably at ~1600 cm^{-1} during graphite amorphization [27]. The overall spectra i.e. D band and broadened G band in the spectra of GO-HOPG provides clear indication that GO sheets are present at HOPG substrate.

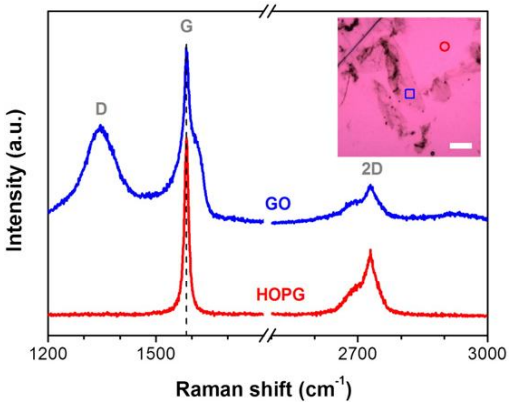

Fig. 1. Comparison of Raman spectra for GO sheets deposited on HOPG and bulk HOPG, recorded with $\lambda_{exc} = 532$ nm. Inset shows the optical image of the GO sheets settled down on HOPG substrate. The location of Raman spectra of GO (square) and HOPG (circle) are indicated in the figure.

4.2. AFM study of graphene oxide sheets on HOPG

An extensive dAFM study was performed for the characterization of GO sheets deposited onto an HOPG substrate. Fig. 2(a) shows a GO sheet supported on a cleaved HOPG substrate. The absence of any wrinkle or fold as well as underlying atomic steps on the HOPG substrate are clearly evident. These features allow an identification of this flake as flat GO. Fig. 2(b) shows a dAFM phase image that confirms that GO is chemically distinct from the supporting HOPG substrate. Smaller flakes present in the image also show the same phase contrast, suggesting they can also be identified as GO. GO sheets of mean area 1.5 μm^2 were obtained on regular basis.

It is possible during deposition that a thin GO sheet may not conformally coat the substrate. This lack of conformality appears as wrinkles in the supported GO sheet. The evidence of wrinkles can be clearly identified from the dAFM images after deposition of GO and this wrinkled morphology is more likely to be observed than a flat morphology. Fig. 3(a) is a typical topographic image of a GO sheet where wrinkles can easily be seen. Height profiles indicate the wrinkles in Fig. 3 have a three dimensional structure that arises due to non-planar deposition. These wrinkles have variable height from 1.0 nm to 4.5 nm above the GO sheet. Fig. 3(a) and (b) are a topographic and phase image, respectively, of the GO sheet. Again, the clear phase contrast between GO and HOPG is evident.

From Fig. 3(b), an average phase difference of 5.5° can be determined as shown in Fig. 3(c) which is a histogram plot of the number of pixels a given phase is recorded in the phase image. Careful examination of Fig. 3(b) also shows a finer phase contrast between the wrinkles and the flatter regions of the GO. Since phase contrast ultimately reflects energy loss between the tip and substrate, it can be concluded that the tip dissipates more energy when intermittently contacting GO as compared to HOPG. Furthermore, the phase contrast across the wrinkles indicates additional energy loss channels become operative when the AFM tip contacts the GO wrinkles. Observed phase shift can be explained by dissipation of energy due to tip-sample interaction. Phase in AFM image is highly influenced by Young's modulus and presence of damping at the surface. In presence of damping, higher Young's modulus material shows bigger phase angle

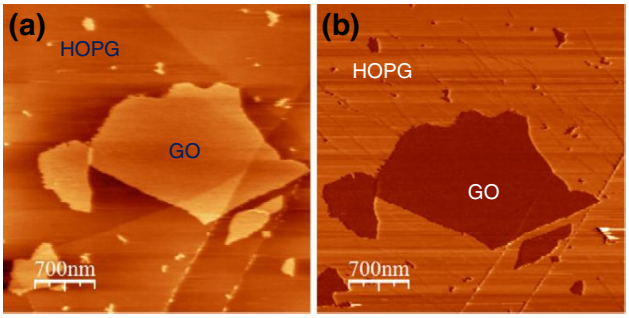

Fig. 2. In (a) Topographic image of GO sheet on top of HOPG substrate. In (b) dAFM phase image showing clear contrast between GO and underlying HOPG substrate.

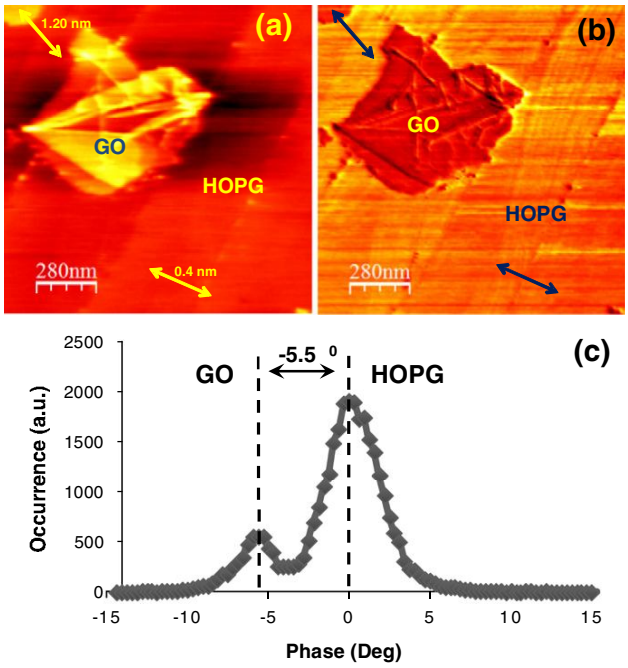

Fig. 3. A typical dAFM topographic image of GO on an HOPG substrate. Prominent wrinkling, presumably related to the deposition of GO, is observed. In (a), an image of approximately $1\times1\,\mu m^2$ GO sample. In (b), a true phase image illustrating folds and wrinkles in the deposited GO sheet. In (c), a phase difference histogram of the dAFM image in (b) shows a 5.5° phase difference between GO and HOPG.

[28]. Considering that tip is primarily attracting at the surface of HOPG, this observed phase difference can be explained by comparing Young's modulus of GO (~230 GPa) [29] with that of graphene (~1 TPa) [30,31]. Considering presence of damping at the surface there is a clear indication of lower phase for GO than HOPG. This result is also consistent with the higher friction observed on GO as compared to HOPG [19,32].

Due to damping and friction of GO, the adhesion of the AFM tip to GO should be greater than on HOPG [28]. To verify this, lift-off measurements under dry nitrogen conditions were made as shown in Fig. 4. A threefold increase in the adhesion force on GO as compared to HOPG suggests that the nature of the tip sample interaction on GO is larger than that of over HOPG.

Evidence of folding of GO sheets upon deposition were also observed in this study. Fig. 5 shows a typical dAFM image of an GO sheet folded onto itself. Fig. 5(a) is a topographic image of GO on HOPG, while Fig. 5 (b) is a phase image that confirms that the sheet shown in Fig. 5(a) is GO. Fig. 5(c) shows a magnified topographic image of the fold in the GO sheet. It is clear from Fig. 5 (b) that there is very little phase contrast between the top and bottom of the folded GO sheet, indicating uniform functionalization on both sides of the GO.

It is further evident that the folded region is torn from the GO sheet. Previous studies have shown that when a graphene sheet folds or tears, it tends to fold or tear along a high symmetry direction (i.e. it can fold at an angle of 30°, 60° or 120°) determined by the underlying hexagonal mesh of carbon atoms [33–35]. Our study shows that GO also preferentially folds or tears at angles that are similar to those found in graphene.

The folding angle of a GO flake can be uniquely defined by first identifying the longest sheet edge that intersects the fold of interest. In Fig. 5 (c), the relevant GO edge is denoted by the line marked $\alpha\delta$. The folding axis is defined by the line marked as $\beta\gamma$, the line that passes through the fold. The folding angle is defined as the angle subtended between the folding axis and the relevant sheet edge. A unique folding angle can always be defined by imagining a restoration of the folded flap to its original position. The folding angle is then defined as the subtended angle that forms between the edge that is *approached* by unfolding and the folding axis.

In Fig. 5(c), the relevant folding angle measured with respect to the GO edge is $\angle\delta\beta\gamma = 60^{\circ}$. The tearing angle is measured by defining a tearing axis, which is simply a line drawn through the tear. The tearing angle is defined as the angle subtended by the same edge used to measure the folding axis and the tearing axis. As can be seen in Fig. 5(c) the tearing angle is $\angle\beta\beta'\gamma' = 120^{\circ}$. As the tear progresses, the tearing angle deviates from the 120° value, indicating a non-uniform tear in the GO sheet. Careful analysis of this image indicates that the area of the folded GO sheet does not match the area of the void from where the sheet has been torn. We conclude that the folded GO sheet is stretched in the process of tearing.

Examination of the image along the folding axis suggests it acquires the shape of a circular bend having a diameter of 2.75 nm as judged by the height of the fold above the HOPG substrate. Although the lateral dimension of the bent region is distorted by tip dilation effects, the diameter of the bend can be accurately identified from the dAFM image. The bend in the GO sheet resembles a graphene oxide nanotube (GONT) which would have a radius of curvature of 1.38 nm.

4.3. STM study of graphene oxide sheets on HOPG

In order to improve the resolution of the relevant features in folded GO sheets deposited onto an HOPG substrate, extensive STM characterization was performed as well. Overall, the results obtained

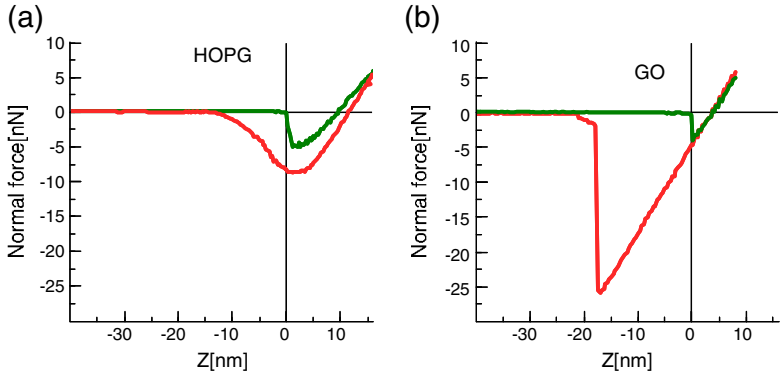

Fig. 4. Typical F(z) data from (a) HOPG and from (b) GO. For the same tip, the lift-off force from GO is ~3 time greater than for HOPG. In both the images green and red curves represents the forward and backward motion of the tip in contact mode, respectively.

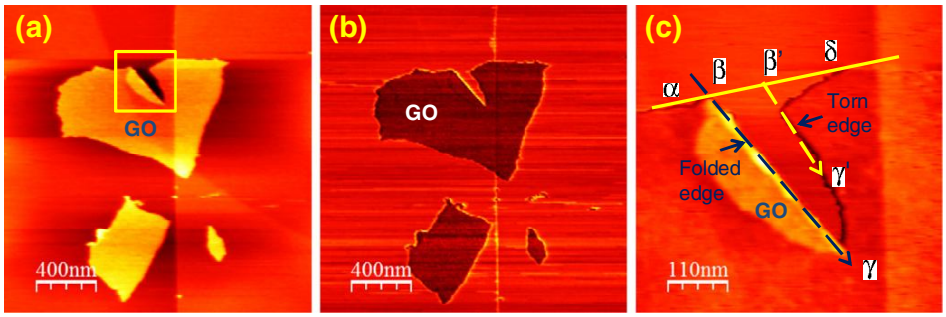

Fig. 5. A typical dAFM topographic image of GO on an HOPG substrate. Prominent folding, presumably related to the deposition of GO, is observed. In (a), an image of approximately $2\times2\ \mu m^2$ GO sample. In (b) a phase image confirming the presence of GO on HOPG. In (c), a magnified image from the selected square region of (a).

by STM were similar to those obtained during the dAFM portion of our study. In the following section, we focus on regions of folded GO sheets after deposition. When using STM, we lose the ability of phase imaging as an identifier of GO. Instead, we now use the thickness of a sheet as a GO identifier. Prior AFM work has shown that the thickness of one GO sheet is approximately 1.1 ± 0.2 nm [12,19] as compared to the expected height of a single graphene sheet in HOPG of 0.34 nm. The increased thickness of a single sheet of GO is attributed in part to its functionalization on both sides as well as subtle differences in how the tip interacts with a thin GO sheet supported on HOPG.

Evidence for folds in deposited GO was also observed in STM images that match well with the folds obtained in our dAFM studies. Fig. 6 shows an STM image of a folded GO sheet supported on an HOPG substrate. As seen in Fig. 6(a), relevant features are marked as HOPG, 1 L GO and 2 L GO. The corresponding z heights are also indicated. The

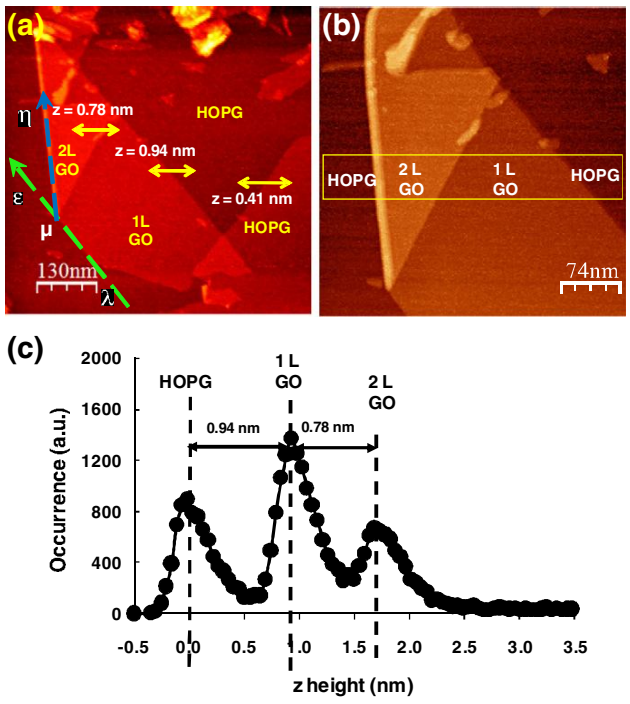

Fig. 6. Typical topographic image of GO on HOPG obtained by STM. Prominent folding of an GO sheet is observed. Flakes of GO are also evident near the top of the image. In (a), an STM image of a 300 nm × 300 nm GO sheet deposited on HOPG. In (b), magnified STM topography image of a region from Figure (a) depicting folded GO on HOPG. In (c) a z-height histogram of the yellow rectangular (color online only) boxed region of the STM image in (b). From the histogram data of (c), a value for the height of one layer of a GO sheet is inferred to be 0.94 nm; the diameter of the fold is 2.88 nm.

height of a step on the HOPG substrate is found to be 0.4 nm. The step height of 0.94 nm represents one GO layer supported on the HOPG substrate. The step height of 0.78 nm represents a second GO layer resting on top of a folded GO sheet. The apparent decrease in the second layer thickness of GO might reflect a decrease in the Local Density of States (LDOS) rather than a decrease in the GO sheet thickness. For an STM operating in constant current mode, the tip-substrate separation is largely determined by variations in the LDOS. It follows that if the tip encounters a region of the substrate with a reduced LDOS, the tip-substrate separation must decrease in order to maintain a constant set-point current. Although it can be argued that a uniformly oxidized sheet of graphene is insulating, non-uniform oxidation or trapped ions may form a sufficiently conducting channel to allow STM measurements. When the tip is positioned over a two layer region of GO, a reduced conduction is likely to cause an apparent decrease in the thickness of the second GO layer in order to maintain a constant set current. This argument provides a qualitative explanation for the step height measurements found in Fig. 6(a). These height measurements allow us to identify the HOPG and GO regions in STM images with confidence.

To characterize the folding axis, the relevant GO edge is identified by the line $\varepsilon\mu\lambda$ and the folding axis is indicated by the line $\mu\eta$. The folding angle is given by $\angle\varepsilon\mu\eta = 30^{\circ}$. Along the folding axis, the GO sheet forms an GONT-type bend with a diameter of approximately 2.9 nm. Fig. 6(c) is a histogram of the topography from the boxed region of Fig. 6(b). The three peaks in the histogram represent the relative height of the HOPG substrate (0.0 nm), the thickness of the folded GO sheet (0.94 nm), and the thickness of two GO sheets (1.72 nm). Height measurements from Fig. 6(b) indicate the diameter of the bend in this GO sheet is 3.07 nm.

We have encountered that some of the GO sheets acquire different morphology than folded GO sheets when deposited onto HOPG substrate. This observation is shown in Fig. 7 and we call it cracking of GO sheet in the process of folding. We believe that underlying reason for this is the excess strain developed in bend GO sheet. This is an important observation because it suggests that a fold in graphene may eventually crack if it slowly oxidizes under ambient conditions. To the best of our knowledge, such cracking of a GO sheet has not been reported to date. Fig. 7 shows an STM topographic image of a GO sheet that cracked in the process of folding. Fig. 7(a) clearly indicates the presence of underlying HOPG steps and a large sheet of GO that conformally covers the underlying HOPG substrate. It can be seen from Fig. 7(a) that the folding axis is $\beta\eta$ and the folding angle is $\angle\gamma\beta\eta = 60^{\circ}$ In contrast to the results shown in Fig. 7, the bent region of the GO does not form a continuous bend. Instead, a well developed crack is observed along the folding axis. It is notable that the crack axis is uneven, suggesting an irregular propagation of the crack upon folding.

Once again GO was differentiated from HOPG by a height difference. The topographic image given in Fig. 7(b) is from the boxed region in Fig. 7(a). A height histogram of this image is also provided and shows three features which clearly correspond to two

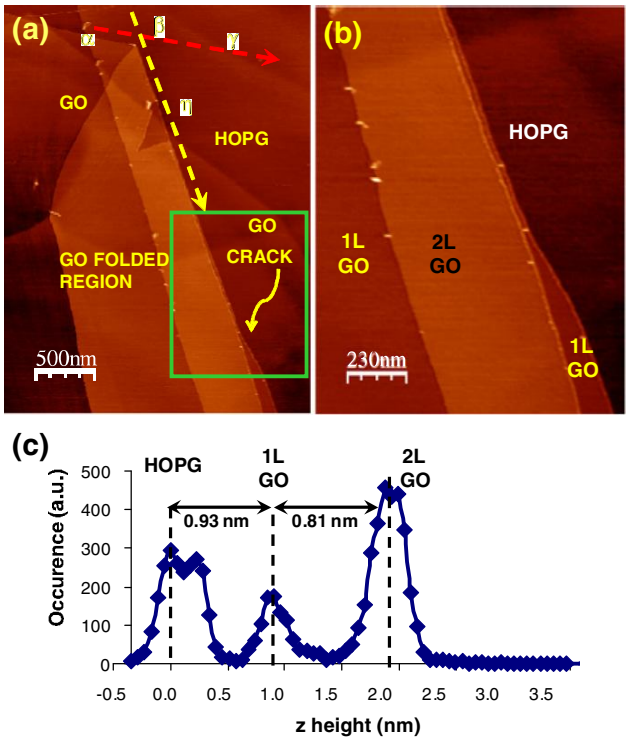

Fig. 7. Typical topographic image of GO on an HOPG substrate obtained by STM. Prominent breaking, presumably related to the deposition of GO, is observed. In (a), an image of a $2.6\times2.6\ \mu m^2$ GO sample. In (b), STM topography image of boxed region depicting cracked GO on HOPG In (c), a z-height histogram of the boxed region of the STM image in (b) which shows the height of two GO atomic steps that are formed due to the cracking of GO in the process of folding.

planes of GO resting on top of the HOPG substrate. Fig. 8(a) shows further details of the crack in GO, using an inverted grey color scheme to enhance the contrast. Fig. 8(b) shows the crack near the top edge of the GO sheet. Fig. 8(c) shows the uneven propagation of the crack edge. The enhanced lateral resolution of STM is critical for resolving the crack in GO that develops upon folding. The uneven nature of the crack edge is a significant departure from the straight line folds that develop when GO folds without cracking. Similar straight line folds are observed when the top layers of graphene fold to make a flap on an HOPG substrate.

5. Discussion

The above studies show that when bent, GO can form either a continuous bend, resembling a GONT structure, or a crack along the folding axis. To gain insight into the cracking of a GO sheet, it is worthwhile to analyze the energetics of folding and tearing in graphene [34–37].

Fig. 9 is a diagram of a graphene sheet with the high symmetry directions indicated by a solid ($[11\bar{2}0]$) or dashed ($[1\bar{1}00]$) lines. For a defect free graphene sheet, there are two families of high symmetry folding axes, namely the $[11\bar{2}0]$ and $[1\bar{1}00]$. Calculations of the energy required to wrap nanotubes around these two axes indicate that the energy required for wrapping a nanotube around $[11\bar{2}0]$ is 0.38 eV/atom lower than for wrapping around $[1\bar{1}00]$[33,37]. This result is consistent with an experimental AFM study showing that the preferential folding axis for a graphene sheet is found to be $[11\bar{2}0]$[33]. This axis passes through two carbon atoms for each hexagonal ring, making it easier to form a small bend because the bending axis is parallel to all bonds. Folding around any other axis will cause dihedral bond bending and hence a distortion of the hexagonal network, thus increasing the stored energy. Taken together, these considerations suggest that the most probable folding axis of a graphene sheet deposited from solution onto a susbtrate is $[11\bar{2}0]$.

Prior to STM studies [33–35] of a folded topmost graphene layer in HOPG do not show cracking but rather a continuous folding along the bend axis. Our studies of folds in the topmost few layers of HOPG are consistent with these prior studies. We have also observed continuous bends in many GO flakes deposited onto HOPG as discussed above. Any cracking of a GO sheet while folding would therefore represent an entirely new phenomenon. We believe that this is what we are observing in Fig. 7 and Fig. 8. The crack that develops in a folded GO sheet indicates that it is possibility of bond failure in the high stress region of GO due to folding. Similar to graphene, it is likely that bending in GO also occurs preferentially about $[11\bar{2}0]$ axis. Cracking is then likely related to the weakening of C–C bonds due to oxidation along $[11\bar{2}0]$.

The functionalization of graphene to make GO introduces defects in the graphene lattice and provides the basis for understanding cracking (bond failing) in GO sheets in the process of folding. To locally oxidize graphene, C atoms become functionalized with carboxyl, hydroxyl, and/or epoxy groups [23,38]. An STM study [19] as well as a theoretical study [39] showed that small regions of GO

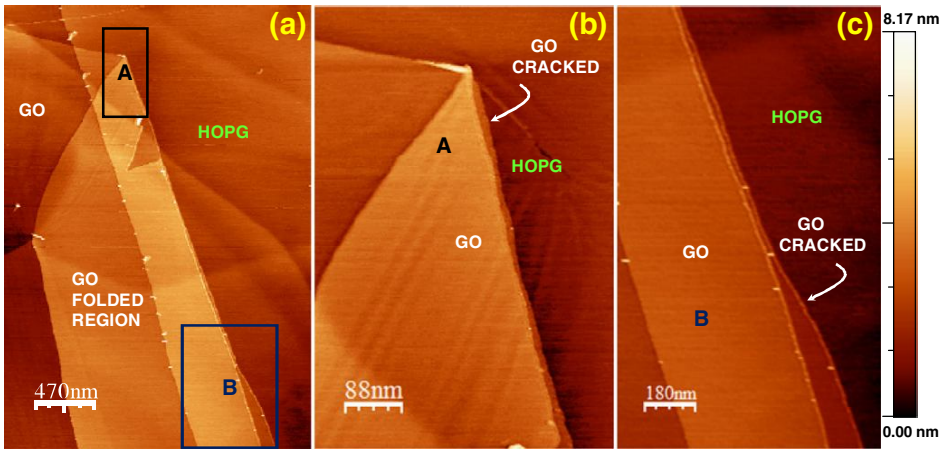

Fig. 8. This figure shows the magnified STM image of crack developed in GO sheet in the process of folding. The height bar at the right of the image shows that dark region is the higher region.

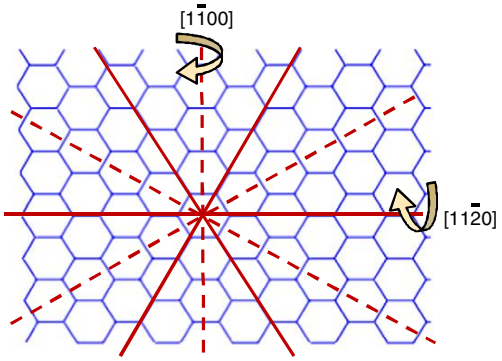

Fig. 9. A sketch of a graphene layer with symmetry axis indicated.

appear to have a periodicity that is consistent with that expected for epoxide bond (C-O-C) formation. Raman studies indicate that the oxidation of graphene proceeds by random functionalization with carboxyl and hydroxyl groups [40–42]. Furthermore, NMR studies indicate that graphene oxidizes in a random fashion on both the top and bottom sides [23,38]. Although detailed atomistic calculation are required to fully understand the implications of graphene oxidation, it seems reasonable to expect that any functionalization, be it random or highly ordered, will locally weaken C–C bonds.

Fig. 10(a) is a schematic of a highly ordered GO sheet. The solid dots represent –O– that forms an epoxide group bridging two C atoms. The $[1\bar{1}00]$ and $[11\bar{2}0]$ directions indicate the orientation of the two high-symmetry folding axes. The number of –O– atoms required for a complete oxidation of a line along $[11\bar{2}0]$ is about one-half that needed along $[1\bar{1}00]$. As discussed above, a favorable bending axis for a graphene sheet is $[11\bar{2}0]$. In GO, the C–C bonds along $[11\bar{2}0]$ will weaken when oxidized, causing a reduction in the bending stiffness about this bending axis. In practice, the oxidation occurs in a random fashion as shown in Fig. 10(b). In this case, the precise direction of the bending axis will be irregular and will take advantage of weakened C–C bonds throughout the GO sheet. As the bend progresses, C–C bond failure occurs due to the excess strain that develops and the reduced C–C bond strength. The breaking of one C–C bond will focus stress along a crack front, further accelerating the failure process. Eventually, the stress that develops while folding will be sufficient to produce a catastrophic failure, resulting in a cracked GO sheet as observed experimentally in Fig. 10(c), demonstrates the more realistic picture where random oxidation occurs due to –O– and –OH groups. Once again, the precise direction of the bending axis shown by the dashed line will be irregular and will take advantage of weakened C–C bonds randomly distributed throughout the GO sheet.

6. Conclusions

Raman study along with STM and dAFM (under dry nitrogen conditions) were used to study the folding of GO as it is deposited from solution onto HOPG. Deposited GO sheets could be readily identified using phase contrast imaging by measuring the height of a single sheet with an STM, or by performing adhesion maps. Our work has focused on

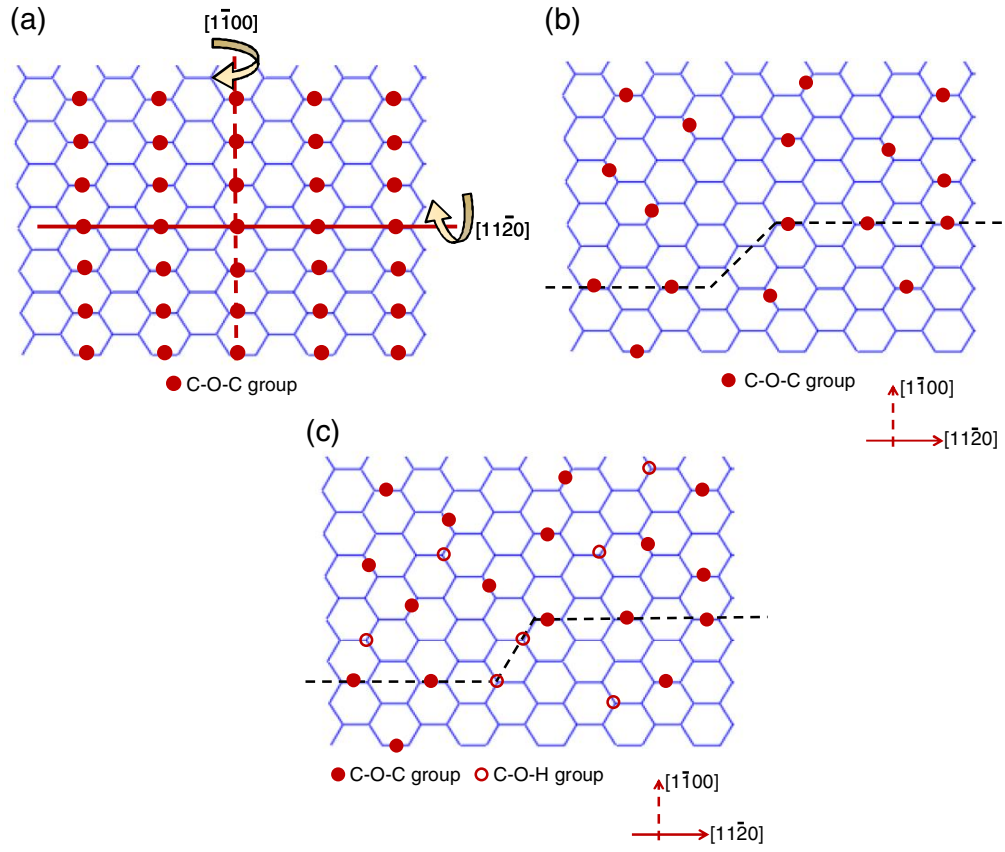

Fig. 10. Schematic of functionalized graphene to form GO. In (a), a schematic of a grapheme sheet with a periodic functionalization by –O– atoms. The high symmetry bending axes are also drawn. In (b), a graphene sheet exhibiting a random functionalization by –O– atoms. The dashed line indicates a weak bending axis that may follow an irregular path to take advantage of the random location of the functionalized graphene. In (c), a graphene sheet exhibiting a random functionalization by both –O– atoms and –OH groups. The dashed line indicates a weak bending axis that may follow an irregular path to take advantage of the random location of both –O– atoms and –OH groups.

the morphology of supported GO sheets after deposition. Both tearing and folding of GO have been observed. Analysis of the measured tearing and folding angles reveal they are similar to those reported in HOPG studies, indicating that folding and tearing preferentially occur along high symmetry directions in the GO sheet.

Unless GO is deposited in a highly controlled fashion so that an GO sheet approaches the underlying substrate in a parallel plate configuration, the deposition will always be characterized by a process in which some edge of the GO makes a first contact to the substrate. Assuming this edge becomes tethered due to van der Waals interactions, the remainder of the GO sheet will twist and bend until it collapses onto the substrate. As a result, deposited sheets can have a crumpled appearance, full of wrinkles. It is also possible that the GO can bend and fold onto itself as it settles onto the substrate. The characteristics of this bending and folding are interesting because they shed light on the mechanical properties of GO.

Our data indicates that when GO sheets fold, the bent region around the folding axis can be described by a high radius of curvature. The bend resembles a CNT-like structure with a measured radius of curvature comparable to those reported for SWCNTs. We call this bent region a GONT. However, it is possible that when a GO sheet folds, a crack can develop along the folding axis. Presumably, this cracking is related to a reduced stiffness attributed directly to the highly functionalized nature of the GO sheet.

It is well established that it is easier to bend a graphene sheet about $[11\bar{2}0]$than around$[1\bar{1}00]$. This result can be attributed to the greater number of bonds that must be deformed when bending about the $[1\bar{1}00]$ axis. For the case of GO, weakening of bonds is expected to occur due to the random functionalization of graphene with O and OH groups. In addition, random vacancies could also further weaken the C–C network. Taken together, this weakening provides a natural explanation for the cracking in the GO sheet during folding.

This work is interesting because it anticipates a failure mode for future graphene electronic devices. Any area of defect-free graphene with a high radius of curvature will be more chemically active than the surrounding flat region. This implies that graphene that is bent or wrinkled will slowly oxidize with time. The oxidation will serve to weaken C–C bonds, and will eventually lead to a crack that propagates and splits the graphene sheet. In the future, it is likely that this failure mode must be countered in order to insure the high reliability of graphene electronics.

Acknowledgements

The GO sample was prepared by Sasha Stankovich working in the laboratory of Rodney Ruoff at Northwestern University (now at the University of Texas). This work was supported by NASA (award # NCC-1-02037) through the University Research, Engineering and Technology Institute (URETI) on Bio-inspired Materials (BiMat).

References

[1] K.S. Novoselov, A.K. Geim, S.V. Morozov, D. Jiang, Y. Zhang, S.V. Dubonos, et al., Electric field effect in atomically thin carbon films, Science. 2004 306 (5696) (October 22, 2004) 666–669.
[2] D.A. Dikin, Sasha Stankovich, Eric J. Zimney, Richard D. Piner, Geoffrey H.B. Dommett, Guennadi Evmenenko, SonBinh T. Nguyen, Rodney S. Ruoff, Preparation and characterization of graphene oxide paper, Nature. 448 (7152) (2007) 457–460.
[3] S. Stankovich, D.A. Dikin, G.H.B. Dommett, K.M. Kohlhaas, E.J. Zimney, E.A. Stach, et al., Graphene-based composite materials, Nature. 442 (7100) (2006) 282–286.
[4] HcA Becerril, J. Mao, Z. Liu, R.M. Stoltenberg, Z. Bao, Y. Chen, Evaluation of solution-processed reduced graphene oxide films as transparent conductors, ACS Nano. 2 (3) (2008) 463–470.
[5] J. Wu, H.A. Becerril, Z. Bao, Z. Liu, Y. Chen, P. Peumans, Organic solar cells with solution-processed graphene transparent electrodes, Applied Physics Letters. 92 (26) (2008) 263302–263303.
[6] J.T. Robinson, F.K. Perkins, E.S. Snow, Z. Wei, P.E. Sheehan, Reduced graphene oxide molecular sensors, Nano Letters. 8 (10) (2008) 3137–3140.
[7] F. Schedin, A.K. Geim, S.V. Morozov, E.W. Hill, P. Blake, M.I. Katsnelson, et al., Detection of individual gas molecules adsorbed on graphene, Nat Mater. 6 (9) (2007) 652–655.
[8] N. Mohanty, V. Berry, Graphene-based single-bacterium resolution biodevice and DNA transistor: interfacing graphene derivatives with nanoscale and microscale biocomponents, Nano Letters. 8 (12) (2008) 4469–4476.
[9] R.D.P. Sasha Stankovich, Chen Xinqi, Wu Nianqiang SonBinh T. Nguyen, Rodney S. Ruoff, Stable aqueous dispersions of graphitic nanoplatelets via the reduction of exfoliated graphite oxide in the presence of poly(sodium 4-styrenesulfonate, J Mater Chem. 16 (2006) 155–158.
[10] G. Eda, G. Fanchini, M. Chhowalla, Large-area ultrathin films of reduced graphene oxide as a transparent and flexible electronic material, Nat Nano. 3 (5) (2008) 270–274.
[11] G. Eda, Y.-Y. Lin, S. Miller, Y. Chen, W.-F. Su, M. Chhowalla, Transparent and conducting electrodes for organic electronics from reduced graphene oxide, Applied Physics Letters. 92 (23) (2008) 233305.
[12] C. Gomez-Navarro, R.T. Weitz, A.M. Bittner, M. Scolari, A. Mews, M. Burghard, et al., Electronic transport properties of individual chemically reduced graphene oxide sheets, Nano Letters. 7 (11) (2007) 3499–3503.
[13] T. Ramanathan, A.A. Abdala, S. Stankovich, D.A. Dikin, M. Herrera Alonso, R.D. Piner, et al., Functionalized graphene sheets for polymer nanocomposites, Nat Nano. 3 (6) (2008) 327–331.
[14] S. Stankovich, D.A. Dikin, R.D. Piner, K.A. Kohlhaas, A. Kleinhammes, Y. Jia, et al., Synthesis of graphene-based nanosheets via chemical reduction of exfoliated graphite oxide, Carbon. 45 (7) (2007) 1558–1565.
[15] H.C. Schniepp, J.-L. Li, M.J. McAllister, H. Sai, M. Herrera-Alonso, D.H. Adamson, et al., Functionalized single graphene sheets derived from splitting graphite oxide, The Journal of Physical Chemistry B. 110 (17) (2006) 8535–8539.
[16] D. Li, M.B. Muller, S. Gilje, R.B. Kaner, G.G. Wallace, Processable aqueous dispersions of graphene nanosheets, Nat Nano. 3 (2) (2008) 101–105.
[17] J.-A. Yan, L. Xian, M.Y. Chou, Structural and electronic properties of oxidized graphene, Physical Review Letters. 103 (8) (2009) 086802.
[18] J. Nakamura, J. Ito, A. Natori, Structural bistability of the oxygen-adsorbed graphene sheet, Journal of Physics: Conference Series. 100 (2008) 052019.
[19] D. Pandey, R. Reifenberger, R. Piner, Scanning probe microscopy study of exfoliated oxidized graphene sheets, Surface Science. 602 (9) (2008) 1607–1613.
[20] H. He, J. Klinowski, M. Forster, A. Lerf, A new structural model for graphite oxide, Chemical Physics Letters. 287 (1–2) (1998) 53–56.
[21] K.A. Mkhoyan, A.W. Contryman, J. Silcox, D.A. Stewart, G. Eda, C. Mattevi, et al., Atomic and electronic structure of graphene-oxide, Nano Letters. 9 (3) (2009) 1058–1063.
[22] H. He, T. Riedl, A. Lerf, J. Klinowski, Solid-state NMR studies of the structure of graphite oxide, The Journal of Physical Chemistry. 100 (51) (1996) 19954–19958.
[23] A. Lerf, H. He, M. Forster, J. Klinowski, Structure of graphite oxide revisited, The Journal of Physical Chemistry B. 102 (23) (1998) 4477–4482.
[24] W.S. Hummers, R.E. Offeman, Preparation of graphitic oxide, Journal of the American Chemical Society. 80 (6) (1958) 1339.
[25] F. Tuinstra, J.L. Koenig, Raman spectrum of graphite, Journal of Chemical Physics. 53 (3) (1970) 1126.
[26] K.N. Kudin, B. Ozbas, H.C. Schniepp, R.K. Prud'homme, I.A. Aksay, R. Car, Raman spectra of graphite oxide and functionalized graphene sheets. Nano Letters. 8 (1) (2007) 36–41.
[27] A.C. Ferrari, J. Robertson, Interpretation of Raman spectra of disordered and amorphous carbon, Physical Review B. 61 (20) (2000) 14095.
[28] L. Wang, The role of damping in phase imaging in tapping mode atomic force microscopy, Surface Science. 429 (1–3) (1999) 178–185.
[29] J.W. Suk, R.D. Piner, J. An, R.S. Ruoff, Mechanical properties of monolayer graphene oxide, ACS Nano. 4 (11) (2010) 6557–6564.
[30] C. Gomez-Navarro, M. Burghard, K. Kern, Elastic properties of chemically derived single graphene sheets, Nano Letters. 8 (7) (2008) 2045–2049.
[31] A. Sakhaee-Pour, Elastic properties of single-layered graphene sheet, Solid State Communications. 149 (1–2) (2009) 91–95.
[32] H.C. Schniepp, K.N. Kudin, J.-L. Li, R.K. Prud'homme, R. Car, D.A. Saville, et al., Bending properties of single functionalized graphene sheets probed by atomic force microscopy, ACS Nano. 2 (12) (2008) 2577–2584.
[33] L.X. Li, R.P. Liu, Z.W. Chen, Q. Wang, M.Z. Ma, Q. Jing, et al., Tearing, folding and deformation of a carbon-carbon sp2-bonded network, Carbon. 44 (8) (2006) 1544–1547.
[34] H.V. Roy, C. Kallinger, K. Sattler, Study of single and multiple foldings of graphitic sheets, Surface Science. 407 (1–3) (1998) 1–6.
[35] H.V. Roy, C. Kallinger, B. Marsen, K. Sattler, Manipulation of graphitic sheets using a tunneling microscope, Journal of Applied Physics. 83 (9) (1998) 4695–4699.
[36] M.B. Nardelli, B.I. Yakobson, J. Bernholc, Brittle and ductile behavior in carbon nanotubes, Physical Review Letters. 81 (21) (1998) 4656.
[37] M. Buongiorno Nardelli, B.I. Yakobson, J. Bernholc, Mechanism of strain release in carbon nanotubes, Physical Review B. 57 (8) (1998) R4277.
[38] T. Nakajima, A. Mabuchi, R. Hagiwara, A new structure model of graphite oxide, Carbon. 26 (3) (1988) 357–361.
[39] J. Nakamura, J. Ito, A. Natori, Structural bistability of the oxygen-adsorbed graphene sheet, Journal of Physics: Conference Series. 5 (2008) 052019.
[40] D.W. Boukhvalov, M.I. Katsnelson, Modeling of graphite oxide, Journal of the American Chemical Society. 130 (32) (2008) 10697–10701.
[41] H.K. Jeong, H.J. Noh, J.Y. Kim, M.H. Jin, C.Y. Park, Y.H. Lee, X-ray absorption spectroscopy of graphite oxide, EPL (Europhysics Letters). (6) (2008) 67004.
[42] H.-K. Jeong, Y.P. Lee, R.J.W.E. Lahaye, M.-H. Park, K.H. An, I.J. Kim, et al., Evidence of graphitic AB stacking order of graphite oxides, Journal of the American Chemical Society. 130 (4) (2008) 1362–1366.